REVIEW OF QG THEORY – PART III
A DIFFERENT APPROACH

David Billingsley

National Weather Service Forecast Office
Boise, Idaho

Editor's note: *This is the third in a series of continuing education articles on QG theory. The first, "What Does Quasi-Geostrophic Really Mean?" was published in the National Weather Digest Volume 21 Number 1. The second, "Review of QG Theory — Part II: The Omega Equation," was published in Volume 21 Number 2. David Billingsley, Science and Operations Officer, NOAA/NWSFO, Boise, Idaho volunteered to author this timely series and his initiative, time and special efforts are deeply appreciated. Supportive comments have been received from many readers.*

1. Introduction

As discussed in part II of this series (Billingsley 1997), diagnosis of large scale vertical motion via the traditional omega equation is often difficult due to the potentially opposing terms (differential vorticity and temperature advection). In the late 1970s, Hoskins et al. (1978) and Trenberth (1978; also see Sutcliffe 1947) provided two alternative approaches whereby the forcing functions on the right-hand side of the omega equation were consolidated into one term. By using either method, forecasters could evaluate a single term and qualitatively deduce the sign of vertical motion without the potential ambiguity inherent in the traditional omega equation.

In short, the Hoskins approach relates the divergence of Q-vectors to the vertical motion field while the Trenberth equation shows a proportionality between the vertical motion field and advection of vorticity by the thermal wind. The second approach has become known as PIVA (positive isothermal vorticity advection) or NIVA (negative isothermal vorticity advection) in the operational community. For reference, the traditional and the two alternative forms of the omega equation are shown below:

Traditional

$$\left(\sigma\nabla_p^2 + f_0^2\frac{\partial^2}{\partial p^2}\right)\omega = -f_0\frac{\partial}{\partial p}\left[-\vec{V}_g\cdot\nabla_p(\zeta_g+f)\right] - \nabla_p^2\left[-\vec{V}_g\cdot\nabla_p\left(-\frac{\partial\phi}{\partial p}\right)\right] \quad (1)$$

(omega ~ differential vorticity advection + thickness advection)

Hoskins et al.

$$\left(\sigma\nabla_p^2 + f_0^2\frac{\partial^2}{\partial p^2}\right)\omega = -2\nabla_p\cdot\vec{Q} \quad (2)$$

(omega ~ divergence of Q-vectors)

Trenberth

$$\left(\sigma\nabla_p^2 + f_0^2\frac{\partial^2}{\partial p^2}\right)\omega = f_0\left[2\left(\frac{\partial\vec{V}_g}{\partial p}\cdot\nabla_p\zeta_g\right)\right] \quad (3)$$

(omega ~ advection of vorticity by thermal wind)

Cursory examination of the three equations quickly yields a common theme:

Laplacian of ω = forcing function/s

In even simpler terms, each equation relates omega to a forcing function on the right-hand side. Since the left-hand sides of eqns. 1-3 are identical, the discussion in article II of this series relating the proportionality of omega and the Laplacian of omega applies equally well to both Hoskins' Q-vector method and Trenberth's PIVA/NIVA approach. For example, it was shown that the larger scale areas of forcing dominated the sign of the omega field, even away from the center of forcing. That is, a large and strong area of positive differential vorticity advection would likely control the sign of omega even in nearby areas of weak negative differential vorticity advection (neglecting the effects of temperature advection). In the same sense, a larger scale, strong area of Q-vector convergence could control the sign of omega even in nearby areas of weak Q-vector divergence. Similar statements can be made about the Trenberth forcing function.

Readers should note that the traditional omega equation displayed at (1) is slightly different from the omega equation shown in the second installment of this series (see eqn. 1 in Billingsley 1997). Both sides of the second article's eqn. 1 have been multiplied by the static stability parameter resulting in (1) here. This slight revision allows for the separation of the static stability parameter and the forcing functions on the right-hand side which simplifies interpretation of all three versions of the omega equation discussed in this paper.

The three methods will typically produce the same qualitative pattern of forcing for a given synoptic situation (Fig. 1). The traditional omega equation and the Q-vector formulation are exact in comparison, i.e., the right-hand sides are mathematically equivalent. On the other hand, the Trenberth approach is derived at the expense of some deformation terms which are neglected in the result. These deformation terms may be important near lower-tropospheric fronts and upper-tropospheric jet

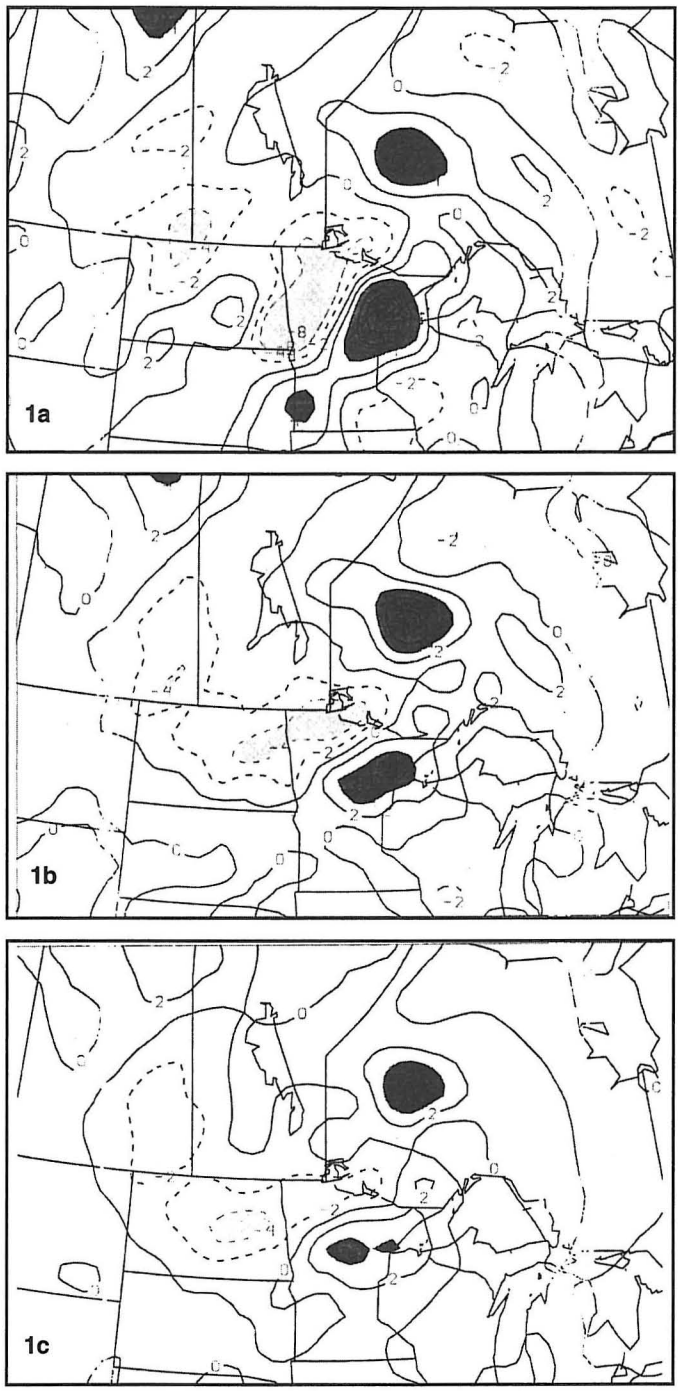

Fig. 1. Right hand side forcing values from the (a) traditional omega equation, (b) the Q-vector formulation, and (c) the Trenberth method (see eqns. 1-3 in text). Dark (light gray) shading implies upward (downward) motion. Forcing is calculated in a layer near 500 mb. Contour interval is 2 x 10^{-15} mb^{-1} s^{-3}.

streaks. More recently, evidence suggests that the magnitude of these deformation terms is also significant in the middle troposphere near the occluded quadrant of a post-mature cyclone (Martin 1998). Hence, qualitative discrepancies are possible when comparing PIVA/NIVA with the Q-vector and traditional approaches near these features. It is interesting to note that despite the mathematical equivalency of the traditional and Q-vector methods, the Q-vector and PIVA examples in Fig. 1 (cfs. 1b and 1c) are more qualitatively similar than are the Q-vector and traditional methods (cfs. 1a and 1b). This apparent contradiction is likely due to the finite difference approximations used to calculate the derivatives in each equation.

Another similarity among the three methods concerns the relationship between the forcing functions and the static stability. It was shown in article II that an inverse relationship exists between the static stability of an airmass and the degree of forcing necessary to produce vertical motion. This relationship is also valid for the forcing functions of (2) and (3) above. As a result, Q-vector convergence or PIVA should be more efficient at producing upward motion in areas that are less statically stable than in a more statically stable environment. This suggests that some measure of static stability should be incorporated as well in the alternative methods of diagnosis.

The subtle, but important point of this discussion is that all three approaches above are based in quasi-geostrophic theory. Assumptions used to arrive at the traditional omega equation limit its application to significant synoptic-scale systems. This statement is equally valid for the application of Q-vector divergence and PIVA/NIVA in diagnosing vertical motion.

2. What is a Q-vector?

Most forecasters understand that the convergence of Q-vectors is proportional to synoptic-scale vertical motion. It is the concept or physical description of a Q-vector itself that is more difficult to comprehend. The easiest way to "de-mystify" the Q-vector is to break it down into simple terms and investigate its physical representation on a term-by-term basis. To accomplish this goal, the Q-vector must be defined mathematically:

$$\vec{Q} = Q_1 \hat{i} + Q_2 \hat{j} \tag{4}$$

where

$$Q_1 = -\frac{R}{p}\left(\frac{\partial \vec{V}_g}{\partial x} \cdot \nabla_p T\right) \tag{5}$$

$$Q_2 = -\frac{R}{p}\left(\frac{\partial \vec{V}_g}{\partial y} \cdot \nabla_p T\right) \tag{6}$$

Looking at the two components of $\mathbf{Q}$, it is apparent that the Q-vector has something to do with the horizontal vector wind change components and the temperature gradient (the two terms in the dot product within the parentheses). Expanding Q_1 and Q_2 gives:

$$Q_1 = -K\left[\frac{\partial}{\partial x}\left(u_g\hat{i} + v_g\hat{j}\right)\cdot\frac{\partial T}{\partial x}\hat{i} + \frac{\partial T}{\partial y}\hat{j}\right] = -K\left[\underbrace{\frac{\partial u_g}{\partial x}\frac{\partial T}{\partial x}}_{A} + \underbrace{\frac{\partial v_g}{\partial x}\frac{\partial T}{\partial y}}_{B}\right] \tag{7}$$

$$Q_2 = -K\left[\frac{\partial}{\partial y}\left(u_g\hat{i} + v_g\hat{j}\right)\cdot\frac{\partial T}{\partial x}\hat{i} + \frac{\partial T}{\partial y}\hat{j}\right] = -K\left[\underbrace{\frac{\partial u_g}{\partial y}\frac{\partial T}{\partial x}}_{\mathbf{C}} + \underbrace{\frac{\partial v_g}{\partial y}\frac{\partial T}{\partial y}}_{\mathbf{D}}\right] \quad (8)$$

where

$$K = \frac{R}{p}$$

For purposes here, K will be treated as a constant. The focus will be on the right-hand side terms (**A**, **B**, **C**, and **D**). By aligning isotherms in a certain orientation and by assuming certain geostrophic wind configurations, the terms can be examined in isolation.

Consider the temperature and geostrophic wind fields as shown in Fig. 2. These two diagrams are constructed so that terms **B**, **C**, and **D** are all zero. First, no temperature gradient exists in the y-direction, so that terms **B** and **D** are set to zero. Second, the u-component of the geostrophic wind does not vary in the y-direction, leaving term **C** equal to zero. Hence, term **A** can be evaluated in isolation and the Q-vector will be defined by Q_1:

$$\vec{Q} = Q_1\,\hat{i} = -K\,\frac{\partial u_g}{\partial x}\,\frac{\partial T}{\partial x}\,\hat{i} \quad (9)$$

Temperatures increase to the right or in the positive x-direction in both diagrams, so that $\partial T/\partial x$ is positive. In Fig. 2a, the u-component of the geostrophic wind decreases to the right or in the positive x-direction making $\partial u_g/\partial x$ negative. The right-hand side of (9) is positive, resulting in a positive Q_1 with a direction defined by the i unit vector. Thus, the Q-vector in 2a points in the positive x-direction toward the warm air. In Fig. 2b, the geostrophic wind field is reversed, so that $\partial u_g/\partial x$ is positive. The Q-vector points in the negative x-direction toward the cool air.

Physically, it is easy to imagine the winds in Fig. 2a promoting frontogenesis, i.e., the flow has a tendency to pack the isotherms more closely. The diagram is suggestive of convergence, but remember that a geostrophic wind field is nearly non-divergent. In this case, frontogenesis is being forced primarily by geostrophic deformation (Fig. 3). In Fig. 2b, the geostrophic winds point away from the center of the diagram suggesting frontolysis, or a weakening of the temperature gradient. The deformation pattern has simply been shifted by 90°. In short, the configuration in Fig. 2 is a simple example of a general result:

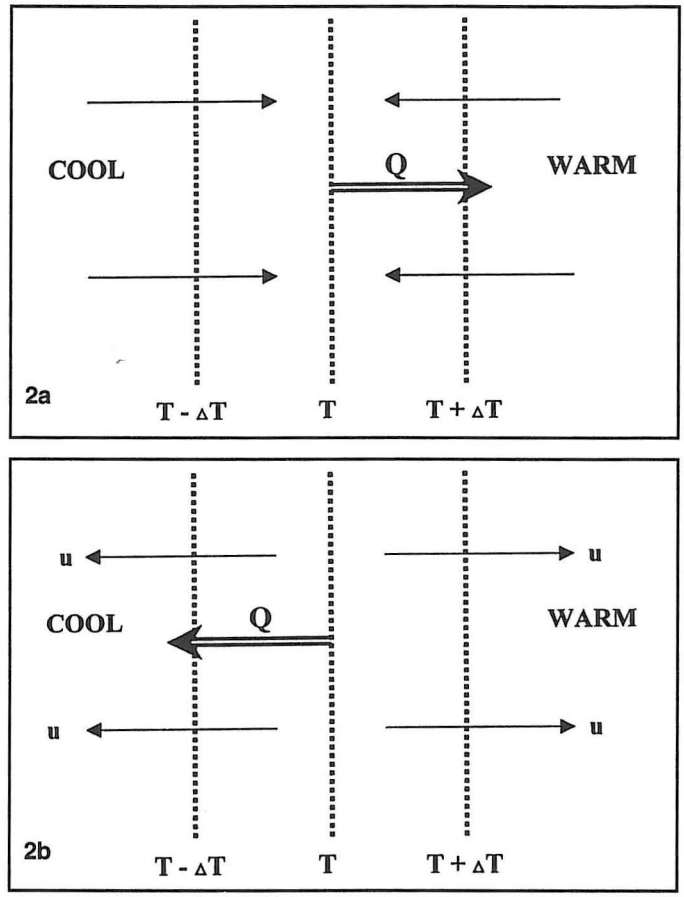

Fig. 2. Conceptual diagrams demonstrating orientation of Q from frontogenetical terms in the definition of Q-vectors: (a) implies geostrophic frontogenesis with Q pointing from cold to warm air and (b) implies geostrophic frontolysis with Q pointing from warm to cold air.

- When the Q-vector points from cool to warm air, geostrophic frontogenesis is implied.
- When the Q-vector points from warm to cool air, geostrophic frontolysis is suggested.

What about the remaining terms (**B**, **C**, and **D**)? By rotating the diagrams in Fig. 2 by 90°, term **D** would take on the role of term **A**. The temperature gradient would point in the y-direction and the v-component of the geostrophic wind would then suggest either frontogenesis or frontolysis. In a similar manner,

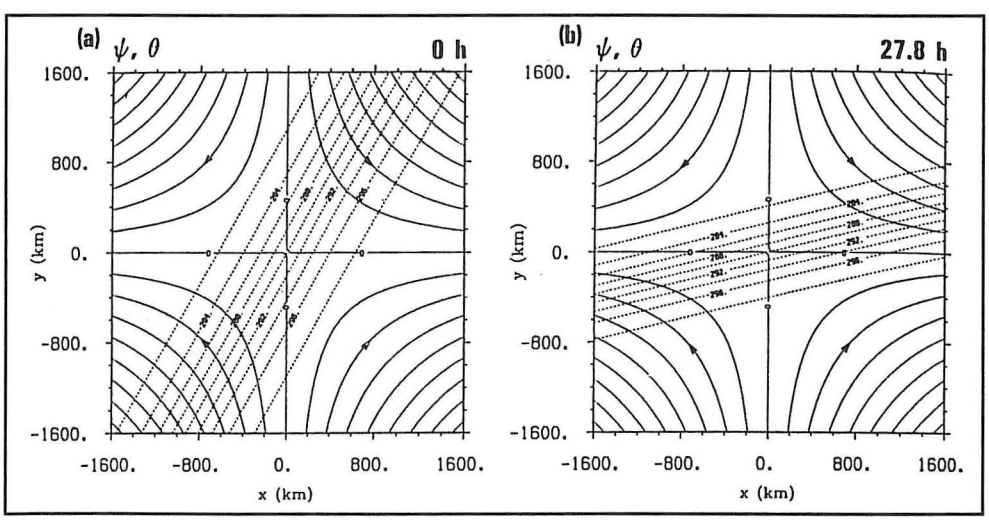

Fig. 3. Figure 2 from Keyser et al. (1988) demonstrating both frontogenesis and rotation of temperature field by deformation. Solid lines represent a streamfunction (velocity) showing pure deformation. Dashed lines are potential temperature (see Keyser text for details).

terms **B** and **C** are related to one physical process (not frontogenesis/frontolysis); only the orientation of the process is different.

Figure 4 exhibits the configuration necessary to demonstrate this other process using term **B**. The figure is constructed so that terms **A**, **C**, and **D** are all set to zero. The Q-vector is determined by Q_1 as follows:

$$\vec{Q} = Q_1 \hat{i} = -K \frac{\partial v_g}{\partial x} \frac{\partial T}{\partial y} \hat{i} \qquad (10)$$

Hence, the Q-vector will point in the positive or negative x-direction. In both diagrams, temperature increases in the negative y-direction, so that $\partial T/\partial y$ is negative in both cases. In Fig. 4a, v_g changes from positive to negative with increasing x, making $\partial v_g/\partial x$ negative. In Fig. 4b, just the opposite is true, so $\partial v_g/\partial x$ is positive. Taking account of all signs, the right-hand side of (10) is negative for Fig. 4a and positive for Fig. 4b. This results in a Q-vector that points in the negative (positive) x-direction for Fig. 4a (Fig. 4b).

From a physical standpoint, it is obvious that no frontogenesis or frontolysis is implied in Fig. 4. That there is not a component of the Q-vector pointing toward cool or warm air is consistent with this result. What is apparent is that the geostrophic wind field is attempting to rotate the isotherms. This rotation can be shown to be the consequence of geostrophic vorticity and deformation (Fig. 3). The only difference in the two diagrams of Fig. 4 is the direction of rotation. Once again, by turning the diagrams by 90° and examining term **C**, the same conclusions would be apparent.

The discussion above might lead to the conclusion that where there is no temperature advection (note the presence of temperature advection in Figs. 2 and 4), Q-vectors are set to zero. This incorrect assumption can be challenged by looking at a third prototype (Fig. 4c). Suppose that the isotherms in a synoptic-scale trough were everywhere parallel to the height contours. Figure 4c would then represent conditions in the base of the trough, i.e., pure westerly flow and a similar temperature gradient as in Figs. 4a and b. No temperature advection is evident in the base of the tough (or elsewhere upstream or downstream). Note that vg is zero; however, $\partial v_g/\partial x$ is positive and $\partial T/\partial y$ is negative just as in Fig. 4b. From (10), **Q** is positive and directed along the x-axis. In fact, **Q** may be strongly positive in such a case.

The absence of temperature advection in Fig. 4c and the description of **Q** as a geostrophic disturbance that deforms the temperature field seems to be contradictory here. The key, in this case, is to define the Q-vector in terms of a geostrophic disturbance that is attempting to change the temperature field within a parcel. As the parcel moves through the trough, the isotherms in the parcel rotate from northwest-southeast on the upstream side to northeast-southwest on the downstream side.

In summary, the Q-vector can be considered representative of a geostrophic disturbance that is attempting to change (deform) the temperature field. If the Q-vector is oriented along the isotherms, the geostrophic disturbance is attempting to rotate the isotherm pattern. If the Q-vector is oriented perpendicular to the isotherms, the disturbance is promoting geostrophic frontogenesis or frontolysis.

3. Q-vectors...Vertical Motion and the Balanced State

How does **Q** relate to synoptic-scale vertical motion? The easy answer is that the divergence of Q-vectors is proportional to the vertical velocity field (see eqn. 2). Where Q-vectors converge (diverge), large-scale upward (downward) motion is inferred (Fig. 1b). Without venturing further, the reader is left with a mathematical construct and no suitable physical explanation. The conceptual picture is at least as important as the tool itself. For this reason, much of this section will dwell on the physical interpretation of the Q-vector field and its relationship to omega and the secondary circulation.

Consider a middle-tropospheric wind maximum similar to what might be found beneath an upper-tropospheric jet streak (Fig. 5). The dominant Q-vector pattern shows **Q** pointing from warm-to-cold air in the exit region and from cold-to-warm air in the entrance region. (The reader can verify the direction of the Q-vectors by looking at **C** and **D** of eqn. 8.) From section 2, it can be deduced that geostrophic frontolysis (frontogenesis) is occurring in the exit (entrance) region. As air moves into the confluent zone (entrance region), one can easily visualize geostrophic advection increasing the temperature gradient. In the exit region, the weakening of the temperature gradient is also evident. These are the effects of the geostrophic disturbance represented by **Q**.

Left with no adjustment, the atmosphere will move out of geostrophic or hydrostatic balance (see part II of

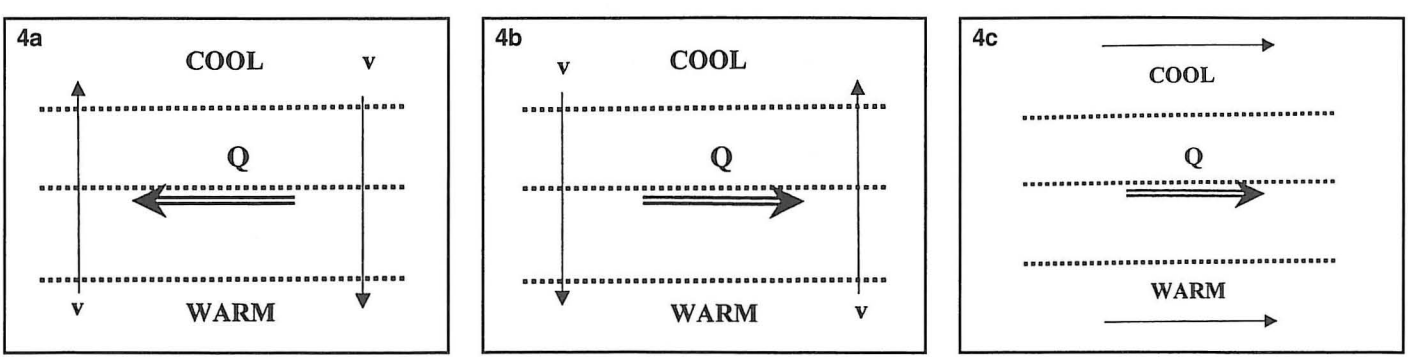

Fig. 4. Similar to Fig. 2, but showing Q contribution to the rotation of the isotherms (thickness contours): (a) and (b) simply show the tendency for anticyclonic and cyclonic rotation respectively: (c) shows a third prototype where isotherms are parallel with geostrophic wind.

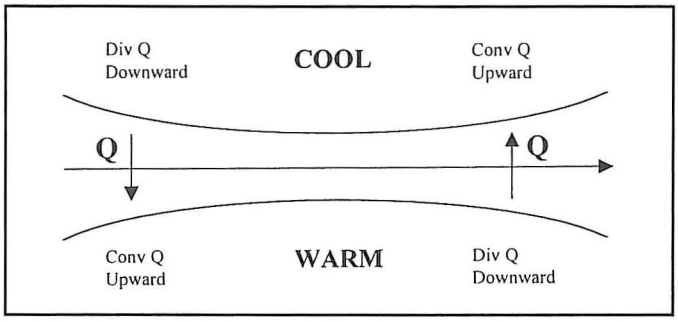

Fig. 5. Simple conceptual model of a straight jet streak showing familiar four-quadrant vertical motion field and association with divergence of Q. Q-vector orientation is shown in the exit (entrance) region promoting geostrophic frontolysis (frontogenesis).

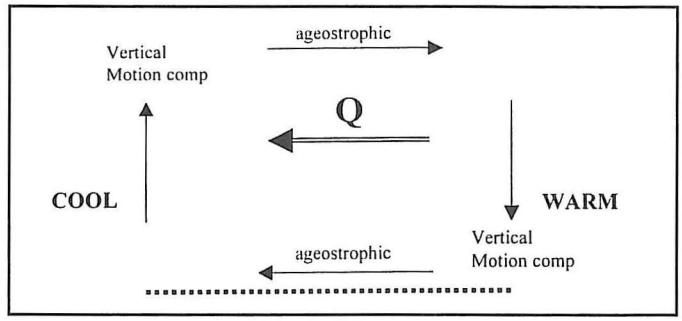

Fig. 6. Cross-section through the exit region of the straight jet streak model. Vertical circulation represents ageostrophic response to the geostrophic disturbance (Q). Note Q is promoting frontolysis while vertical motion branches promote countering frontogenesis (cool air rising and warm air sinking).

this series), or more simply, out of thermal wind balance. In other words, assuming geostrophic and hydrostatic balance are required, a change in the temperature pattern would necessitate a change in the thickness. Thickness changes imply a change in the height pattern which implies a change in the geostrophic wind and so on. Given only a geostrophic disturbance (represented by **Q**) and without any secondary response, the atmosphere would actually move away from geostrophic/hydrostatic balance.

Since QG theory provides a balanced state, the atmosphere does produce a secondary response to achieve this balance. That response is the secondary circulation familiar to most forecasters. For instance, in the exit region, the secondary circulation exhibits an upward branch on the left-front quadrant (Fig. 6) and a downward branch on the right-front quadrant. The corresponding ageostrophic flow in the low levels is from warm to cold air and in the upper levels from cold to warm air. Looking back at the jet streak model (Fig. 5), this configuration is consistent with Q-vector convergence (divergence) in the left-front (right-front) quadrant, assuming a weak Q-vector field surrounding the jet-streak.

How does this secondary circulation help balance the atmosphere? On the cold side of the jet near the exit region (left side of Fig. 6), air is rising, providing additional (adiabatic) cooling. On the warm side, air is sinking, producing additional warming. The combination aids in enhancing the temperature gradient in the region where the geostrophic disturbance (**Q**) is attempting to decrease the temperature gradient. The magnitude of this secondary circulation is just strong enough to keep the atmosphere in thermal wind balance. This secondary circulation in the exit region is termed thermally indirect since cold air is rising and warm air is subsiding. The mirror image of this process can be deduced for the entrance region and is termed a thermally direct circulation.

Another way to look at this process is to remember that the presence of a Q-vector field means that the geostrophic flow is somehow trying to deform the temperature field (see section 2 above). This deformation in the horizontal temperature field necessitates a need for a change in the vertical wind shear (thermal wind equation). However, without going into details, the ageostrophic response associated with **Q** produces the opposite effect; i.e., it decreases the vertical wind shear while increasing the horizontal temperature gradient and vice-versa. The secondary circulation changes the vertical wind shear and the temperature gradient just enough to maintain balance.

It is important to reemphasize that comments about this balance stated in part II of this series apply equally well to the quasi-geostrophic balance discussion using the Q-vector approach. In short, the balance occurs instantaneously; the secondary circulation is not "caused" by the geostrophic disturbance. Moreover, the balanced state says nothing about the future state of the atmosphere. These are diagnostic tools to infer the present state of the synoptic flow.

4. An Illustrative Example

Jet streak conceptual models such as in Fig. 5 are fairly easy to understand. Unfortunately, the atmosphere rarely provides the forecaster with a straight jet streak in an otherwise homogeneous flow pattern. So rather than pick a perfect case study to illustrate the ideas in this paper, a jet streak case was chosen at random. Only the exit region of the jet will be examined due to data cut-off in the entrance region of the data set.

Figure 7 depicts a slightly curved jet streak impending on the Pacific Northwest coast of the United States. Maximum speeds in the jet core are approximately 110 knots. The Q-vector pattern (computed in the mid-levels below the jet) displays a general south to southeast orientation in the exit region immediately off the coast of Oregon and Washington. Cold air is located on the north side of the jet, so this configuration matches the conceptual model in Figs. 5 and 6 fairly well. **Q** is pointing from warm to cold air implying geostrophic frontolysis in this exit region, trying to weaken the temperature gradient. In this case, one would expect a thermally indirect secondary circulation with rising air on the cold side of the exit region and subsiding air on the warm side. The rising air would further cool the cold side and the subsiding air would warm the warm side, resulting in an increased temperature gradient to offset the geostrophic frontolysis.

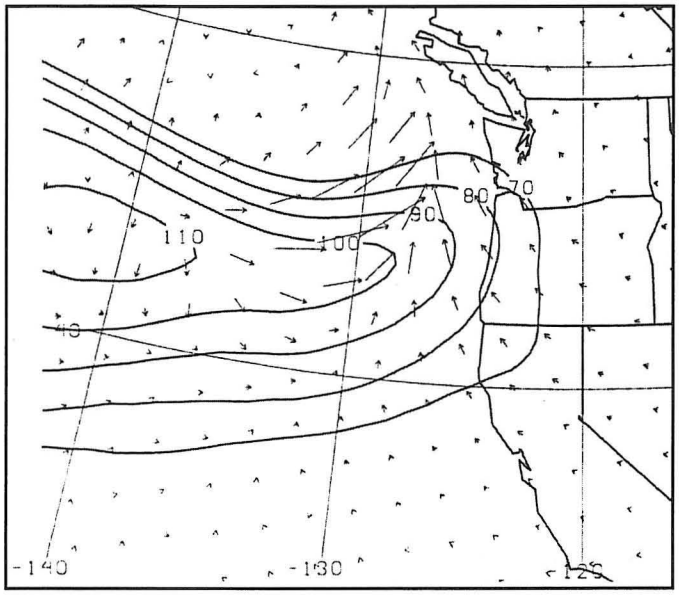

Fig. 7. Q-vectors (arrows) at 500 mb and 300 mb jet (solid) impinging on Pacific Northwest coast from Eta model 48-h forecast valid 1200 UTC 16 April 1998. Q-vectors are scaled and in units of m s^{-3} mb^{-1}. Isotachs contour interval is 10 kts with only 70+ kts shown.

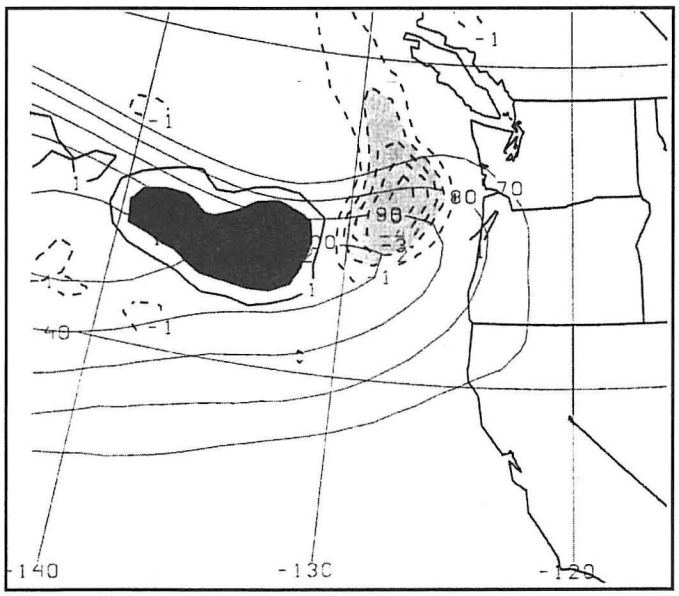

Fig. 8. Q-vector divergence at 500 mb and 300 mb isotachs. Convergence of Q-vectors denoting areas of upward motion are toned in light gray. Divergence of Q-vectors implying downward motion are toned in a darker shade. Q-vector divergence contour interval is 1 x 10^{-15} mb^{-1} s^{-3}.

Does this case demonstrate these ideas? Convergence of **Q** is evident on the north side of the jet (Figs. 7 and 8), suggesting upward motion in this area. A downward motion center (divergence of **Q**), however, is denoted to the west-southwest which is not in the expected location given the straight jet streak conceptual model above (Figs. 5 and 6). Note that the jet possesses cyclonic curvature between the core and the exit region. This configuration translates to a negatively tilted trough at 500 mb with a strong vorticity maximum (Fig. 9) located in the center of the geostrophic disturbance (in the vicinity of the longer Q-vectors). Thus, the pattern in this case is

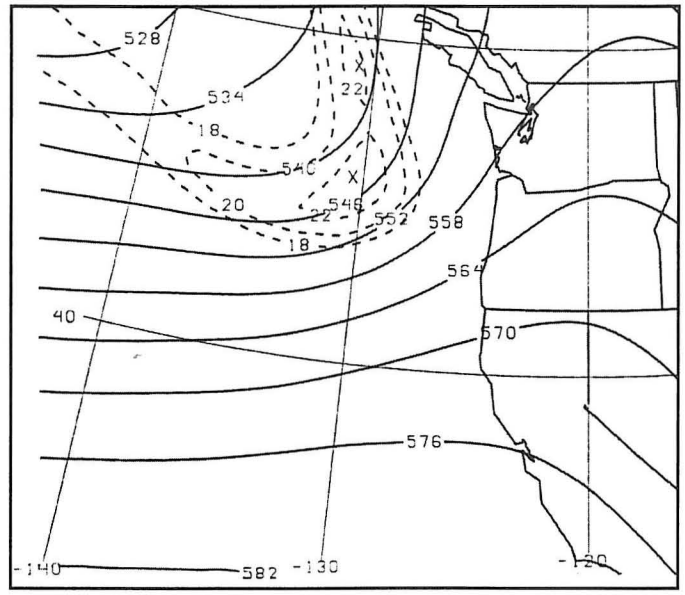

Fig. 9. 500 mb heights (solid) and absolute geostrophic vorticity (dashed). Height contour interval is 60 m. Vorticity contour interval is 2 x 10^{-5} s^{-1} with only values above 18 x 10^{-5} s^{-1} plotted.

quite different from what would be anticipated in the straight jet-streak model.

It is, however, a familiar pattern to forecasters. Typically, with a curved jet (short-wave trough), a dipole or couplet of vertical motion similar to the one shown in Fig. 8 is anticipated with upward motion ahead of the short-wave and downward motion on the upstream side. Theoretically, two circulations can be identified which resolve different scales of forcing (Keyser et al. 1988). The first circulation is parallel to the thickness pattern and denotes the synoptic-scale dipole mentioned above. The second circulation is the familiar transverse secondary circulation in the exit region depicted in the straight jet conceptual model.

To further illustrate these ideas, the Q-vector can be split into components taken parallel and normal to the thickness or isotherm pattern (Keyser et al. 1988, 1992; Barnes and Colman 1993). **Q** becomes:

$$\vec{Q} = Q_s \hat{s} + Q_n \hat{n} \tag{11}$$

where **s** is parallel to the thickness contours with cold air on the left and **n** is normal to the thickness contours in a direction opposite the thickness gradient (pointing toward the cold air side of the jet). Figure 10 demonstrates this orientation using the thickness pattern of the current case study.

In section 2, it was shown that certain terms of **Q** were related to rotation of the isotherm patterns and other terms corresponded to geostrophic frontogenesis or frontolysis. In the simplified examples of Figs. 2 and 4, **Q** was oriented either normal to or parallel with the thickness contours (isotherms). In the former case, frontogenesis or frontolysis was implied as a result of deformation. In the latter case, the resultant wind field appeared to rotate the isotherm pattern.

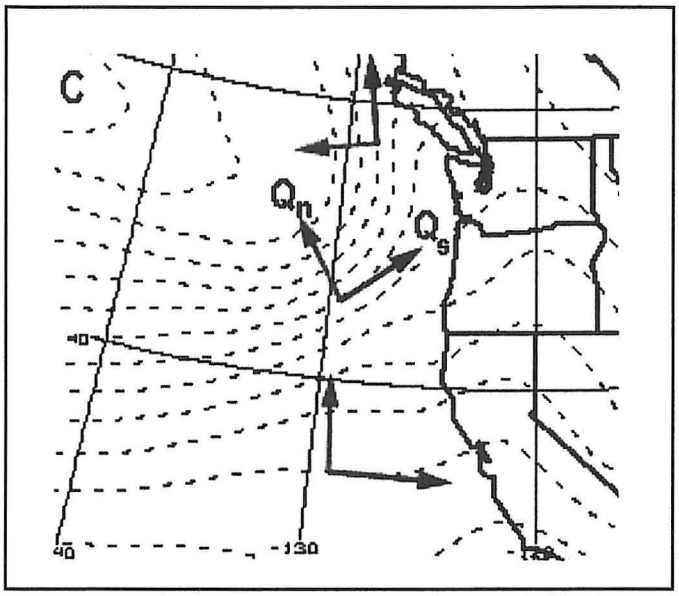

Fig. 10. Conceptual diagram demonstrating orientation of Q_n and Q_s versus thickness contours. Unit vector s is parallel to the contours with cold air on the left and unit vector n is normal to the contours in a direction opposite to the thickness gradient. Light (dark) shaded arrows represent positions of Q_n (Q_s). Cold air is centered in the upper left corner with warmer air to the east and south.

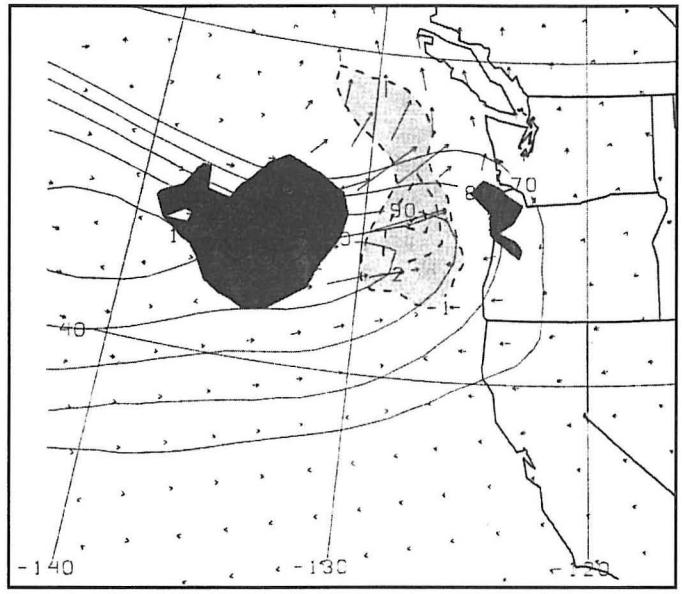

Fig. 11. Q_s-vectors, divergence of Q_s, and isotach pattern. Lighter (darker) shaded regions of Q_s divergence represent upward (downward) branches of secondary circulation. Isotachs are as shown in Fig. 7 and Q_s divergence contours and intervals are shown as in Fig. 8.

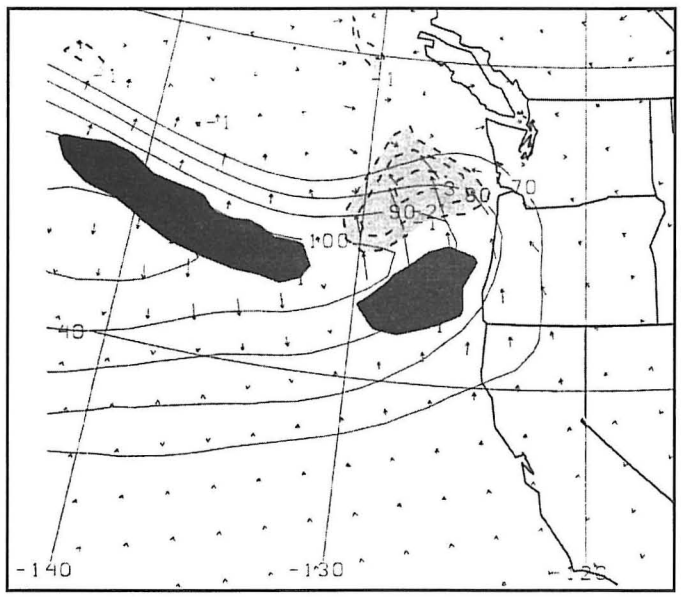

Fig. 12. Q_n-vectors, divergence of Q_n, and isotach pattern. Shading, contours, and intervals as in Fig. 11.

Correspondingly, Keyser et al. (1988) show that Q_n is a function of divergence and deformation of the flow and Q_s is related to the vorticity and deformation of the flow. (Since the flow under our consideration is nearly nondivergent, Q_n can be thought of as simply a function of deformation of the flow.). Following along this line, $\nabla \bullet Q_n$ and $\nabla \bullet Q_s$ relate to circulations normal to and along the thickness pattern, respectively. The $\nabla \bullet Q_s$ circulation is related to rotation of the isotherm pattern by deformation and vorticity while the $\nabla \bullet Q_n$ circulation corresponds to frontogenetical processes associated with the thermally indirect circulation. Keyser et al. (1992) and Barnes and Colman (1993) give evidence that this cross-isotherm flow is related to upper-level frontogenesis and tropopause folding (on a smaller scale than the synoptic dipole associated with Q_s).

In the current case study, Q_s (Fig. 11) and Q_n (Fig. 12) demonstrate some of these ideas. The pattern of $\nabla \bullet Q_s$ appears to be the dominant component of the QG inferred vertical motion field (cfs. 11 and 8). The synoptic dipole of upward-downward motion is quite obvious. A significant portion of implied ascent off the Washington coast, however, is better explained by the thermally indirect circulation denoted by $\nabla \bullet Q_n$ (Fig. 12). Given the proper circumstances, the upward motion branch of this exit region circulation would be watched for evidence of upper level frontogenesis possibly accompanied by bands of precipitation. (A much more detailed case study involving these concepts is contained in Barnes and Colman 1993.)

In summary, the case study shown here does display a thermally indirect circulation as expected, but the curvature of the jet makes it difficult to detect this pattern in the simple divergence of **Q** chart. This secondary circulation is best seen by examining the divergence of the cross-isotherm component of the Q-vector (Q_n) and is associated with the response (frontogenesis) to geostrophic frontolysis. The divergence of the along-stream component (Q_s) helps to depict the familiar synoptic dipole pattern of ascent-descent in an upper-level trough. Its circulation is better related to the rotation of the isotherm or thickness field.

5. What About Trenberth?

Much of the previous discussion is relevant to the Trenberth method shown in section 1. The Q-vector method was discussed in more detail since it is the math-

ematical equivalent of the traditional omega equation. Trenberth's method became popular prior to the advent of significant computer resources in the forecast office. All a forecaster required was a suitable thickness and vorticity chart with overlay capabilities. With the introduction of better computer resources, it is now easy to compute different terms used in QG diagnosis. Since the Trenberth method leaves out some terms that may be important near fronts, jets, and in certain segments of occluded cyclones, it might seem appropriate to suggest abandoning it completely.

6. Summary

Alternative approaches to the traditional omega equation have been discussed with emphasis on the Q-vector approach of Hoskins et al. (1978). A major point of this paper is to remind forecasters that the Q-vector and Trenberth methods are based in the same QG framework as the traditional omega equation. Hence, any assumptions made in the derivation and application of the traditional omega equation are equally valid in the Q-vector and Trenberth approaches. **The use of these diagnostic tools should be limited to synoptic-scale systems.**

The omega equation and the alternative methods are certainly good learning tools and can capture the essence of major synoptic features when used diagnostically. There seems to be, however, some disagreement within the operational community on whether forecasters should continue to utilize QG theory in light of much improved numerical weather prediction models. This issue as well as others will be the focus of the final article (part IV) of this series.

References

Barnes, S.L., and B.R. Colman, 1993: Quasigeostrophic diagnosis of cyclogenesis associated with a cutoff extratropical cyclone - the Christmas 1987 storm. *Mon. Wea. Rev.*, 121, 1613-1634.

Billingsley, D.B., 1997: Review of QG theory - part II: The omega equation. *Natl. Wea. Dig.*, 21:2, 43-51.

Bluestein, H.B., 1992: *Synoptic-Dynamic Meteorology In Midlatitudes, Volume 1.* Oxford University Press, New York, 282-394.

Durran, D.R., and L.W. Snellman, 1987: The diagnosis of synoptic-scale vertical motion in an operational environment. *Wea. Forecasting*, 2, 17-31.

Holton, J.R., 1992: *An Introduction To Dynamic Meteorology*. Academic Press, Inc., New York, 141-180.

Hoskins, B.J., I. Draghici, and H.C. Davies, 1978: A new look at the ω-equation. Quart. *J. Roy. Meteor. Soc.*, 104, 31-38.

Keyser, D., M.J. Reeder, and R.J. Reed, 1988: A generalization of Peterssen's frontogenesis function and its relation to the forcing of vertical motion. *Mon. Wea. Rev.*, 116, 762-780.

_____, B.D. Schmidt, and D.G. Duffy, 1992: Quasigeostrophic diagnosis of three-dimensional ageostrophic circulations in an idealized baroclinic disturbance. *Mon. Wea. Rev.*, 120, 698-730.

Martin, J.E., 1998: On the deformation term in the quasi-geostrophic omega equation. *Mon. Wea. Rev.*, 126, 2000-2007.

Snellman, L.W., 1982: Impact of AFOS on Operational Forecasting. Preprints, *9th Conf. On Weather Analysis and Forecasting*, Seattle, Amer. Meteor. Soc., 13-16.

Sutcliffe, R.C., 1947: A contribution to the problem of development. *Quart. J. Roy. Meteor. Soc.*, 73, 370-383.

Trenberth, K.E., 1978: On the interpretation of the diagnostic quasi-geostrophic omega equation. *Mon. Wea. Rev.*, 106, 131-137.